Chemical Engineering Journal 499 (2024) 156053

Contents lists available at ScienceDirect

Chemical Engineering Journal

journal homepage: www.elsevier.com/locate/cej

Employing a multi-resonance microwave sensor for in-line moisture monitoring of fluidized bed agglomeration

Gero Stoeckl [a,*], Aitor Atxutegi [a], Stefan Bellinghausen [b], Stefan Heinrich [a]

[a] Hamburg University of Technology (TUHH), Institute of Solids Process Engineering and Particle Technology, Denickestrasse 15, 21073 Hamburg, Germany
[b] Siemens, Hammersmith Grove 26-28, London W6 7HA, United Kingdom

ARTICLE INFO

Keywords:
Process monitoring
Fluidized bed
Agglomeration
Process optimization
Sustainable manufacturing

ABSTRACT

Amorphous substances are relatively common in food industry and their characteristics depend highly on the moisture content. Process parameters are adjusted based on online measurements to control the product quality of the agglomerates. This leads to two major challenges: precise moisture content measurements of amorphous particles at (i) different temperatures and for (ii) a wide moisture content range.

In this study two workflows (inline fluidized bed and conditioned fixed bed) calibration of microwave sensors are compared and it is shown that for fluidized beds inline calibration is necessary to achieve accurate moisture measurements. The application of the novel microwave sensor MW 4200 working at resonance frequencies of 2.3 and 5.6 GHz is described. The temperature influence on the measurement is investigated with measurements of a fixed particle bed. Rapid, reliable in-process moisture control at a wide range of moisture contents and temperatures for agglomeration in fluidized beds, with a mean relative accuracy of 82 %, is achieved. This technology improves productivity and precision in industrial operations, minimizes waste and optimizes energy usage.

1. Introduction

Fluidized bed agglomeration is a particle processing method that is frequently used in a variety of sectors and provides a flexible way to have high throughput of particles with specific qualities. Thus, fluidized bed spray granulation and agglomeration are essential processes in the food, fine chemical, and pharmaceutical industries. They allow the production of powders that are free from dust and flow easily, which is important as these properties also influence heat and mass transfer [1,2,3]. Agglomeration is also commonly used in the pharmaceutical manufacturing process for several key purposes, including: (i) enhancing the flowability, porosity and uniformity of powders; (ii) preventing segregation; (iii) regulating the rate of drug release and (iv) minimizing the production of dust [4]. The process affects the product size and removes excess moisture from the particle, enhancing its strength for further handling, such as tableting, which is a key process in the pharmaceutical industry [5].

The size and structure of the final product can be influenced by several factors that also affect the fluid bed agglomeration process itself [6]. Agglomeration refers to the overall process of binding primary particles together to form bigger, porous secondary particles known as agglomerates [7]. A fluid bed granulator is associated with several physical mechanisms occurring simultaneously, including: (i) the atomization of liquid into fine droplets, (ii) the evaporation of droplets, (ii) the deposition of droplets onto the surface of particles, (iii) the drying of the particles and (iv) the formation of agglomerates from wet particles [8,9,10].

Fluidized beds are typically used for granulation, agglomeration and drying of solid materials. It is a widely recognized process that effectively combines these processes in a single step [11]. Due to the empirical development of operating conditions and equipment geometry, the actual influence of fundamental mechanisms in the process (such as wetting of the particle surface and particle interactions) remains little comprehended. Therefore, many unwanted phenomena such as local overwetting or lump formation are common side effects. Overwetting leads to the formation of large particle clusters in the immediate vicinity, while achieving consistent particle growth requires the spray liquid to be evenly dispersed. To predict and avoid overwetting, faster inline measurements are necessary. The moisture distribution within the apparatus also has a significant impact on the size and structure of the final product [12]. The moisture content of the particulate materials also has a significant effect on the particle interactions [13]and the efficiency and effectiveness of agglomeration in a fluidized bed. To obtain the best

* Corresponding author.
E-mail address: gero.stoeckl@tuhh.de (G. Stoeckl).

https://doi.org/10.1016/j.cej.2024.156053
Received 12 July 2024; Received in revised form 4 September 2024; Accepted 20 September 2024
Available online 23 September 2024

Nomenclature

A	Change in resonance frequency. Hz
B	Increase of half width of resonance distribution. Hz
C	Constant
d	Particle diameter. μm
D	Microwave density signal. –
f	Resonance frequency. Hz
k	GT constant. –
m	Sample weight. g
m_m	BET constant. –
n	BET constant. –
r	(Spearman) rank correlation coefficient. –
R^2	Coefficient of determination. –
RH	Relative humidity. –
S	Microwave moisture signal. –
T	Temperature. °C
x_{wb}	Particle moisture content (wet based). wt%
X_{db}	Particle moisture loading (dry based). wt%
Y	Dataset Y
Z	Dataset Z

Latin symbols

α	Water activity. –
ρ	Pearson correlation coefficient. –
σ	Standard deviation

Abbreviations

BET	Brunauer–Emmett–Teller
CFB	Conditioned fixed bed
CFD-DEM	Computation fluid dynamics
DEM	Discrete element method
DoE	Design of experiment
Exp	Experiment
GT	Gordon and Taylor
IFB	Inline fluidized bed
MAPE	Mean average percentage error
MD20	Maltodextrin with dextrose equivalent of 20 wt%
PBM	Population balance model

Subscripts

0	Initial/empty state
f	Filled state
g	Glass transition
s	Solid
w	Water

product quality and process control, precise and real-time moisture monitoring during the fluidized bed agglomeration process is essential.

Offline techniques, which entail routine sampling and analysis of agglomerates, have historically been used to quantify moisture in fluidized bed agglomeration. Although these methods can be quite useful for determining the moisture content of the final product, they are unable to record moisture dynamics and do not contribute to moisture control during the process. The necessity for a non-intrusive, real-time monitoring method that provides continuous moisture measurement within the fluidized bed, enabling precise control and optimization of agglomeration conditions, is therefore urgent. The US Food and Drug Administration released guidelines on process analytical technologies in 2004. These guidelines promote the use of real time measurements during processing, improved process understanding and increased control over industrial processes [14]. Following these guidelines is of highest importance, not only to ensure consistent high product quality but also to avoid increased maintenance and plant shut down, which increases costs and waste.

The development of inline moisture measuring devices, which have the potential to transform the fluidized bed agglomeration process, has been made possible by recent advances in sensor technology [15,16,17,18,19,20,21]. Microwave sensors are an excellent option for in-situ monitoring of moisture dynamics during fluidized bed agglomeration because of their non-intrusive nature. This allows researchers to gain important knowledge on the temporal variation of moisture levels and how it affects agglomerate growth without influencing the process dynamics with the probe position.

The incorporation of a multi-resonance microwave sensor for real-time moisture monitoring of fluidized bed agglomeration is a substantial achievement in the field of sustainable process monitoring. This novel methodology not only improves effectiveness and precision in industrial processing but also conforms to the worldwide necessity for sustainable practices [22]. This method allows for regulation of moisture levels during the agglomeration process, resulting in minimal waste and energy usage, hence reducing the environmental impact. Moreover, its utilization goes beyond just improving efficiency in operations, providing a flexible and adjustable solution that tackles the wider issues of conserving resources, avoiding waste and promoting sustainable industrial growth [22]. This achievement embodies the interplay between technological innovation and environmental care, paving the way for more sustainable industrial processes.

Microwave sensor calibration has made great progress through the development of methodologies that solve the obstacles given by different material properties. The density-independent calibration function allows the precise measurement of moisture contents of granular material [23]. It was shown how versatile microwave sensors are in simultaneously identifying the composition and other aspects of materials, highlighting their suitability for use in intricate settings such as the food industry [24]. Building on these concepts, multivariate calibration techniques were investigated to analyze dielectric spectra directly, thereby increasing the accuracy and adaptability of microwave sensing. These techniques included partial least squares regression and artificial neural networks [25]. By confirming the general applicability across various granular materials of the permittivity-based calibration technique, researchers builton previous research and strengthened the position of microwave sensors as trustworthy instruments for non-invasive material examination [26]. More recently multivariate linear regression was used [19,21] and also combined with principal component analysis [18].

Previous studies have shown that microwave sensors are efficient in evaluating moisture levels in fluidized beds during drying [15] but also layering granulation [19]. These studies generally concentrate on predicting moisture content for single experiments, leading to calibrations that have limited applicability to specific moisture and temperature ranges as a result of a single set of process parameters. Nevertheless, this characteristic restricts their usefulness for ongoing, immediate observation in ever-changing industrial settings where process variables frequently vary. In order to maintain a constant level of quality in the final product, it is necessary to develop calibration methods that are more flexible and can handle a broader range of process parameters. While current literature frequently proposes custom calibrations for specific studies, a more comprehensive approach would entail creating calibrations based on the inherent characteristics of materials. This approach would allow for wider implementation in diverse situations, including varied temperatures and moisture levels, to meet the increasing need for accurate process control and flexible reactor design

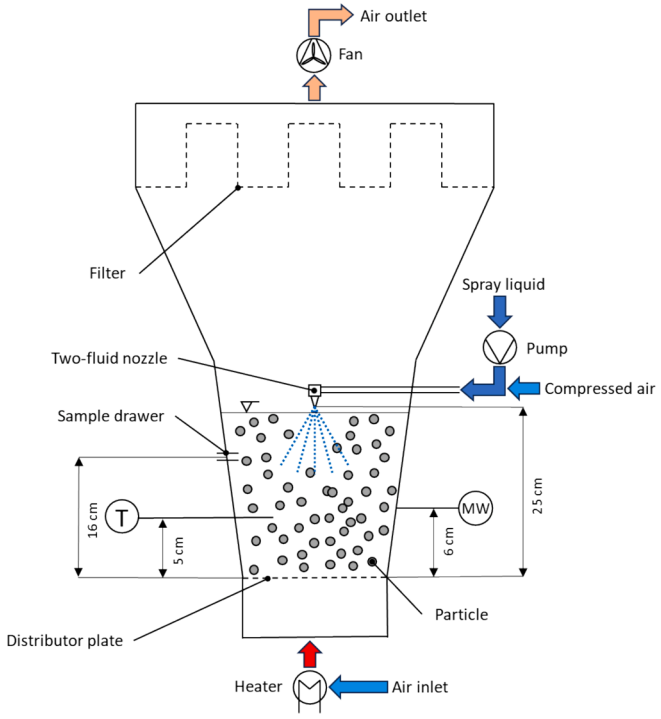

Fig. 1. Scheme of the lab scale fluidized bed setup.

in the industrial sector.

In this study amorphous maltodextrin is used, where the deposited liquid penetrates the surface layer and plasticizes the surface of the particle [27]. This physical mechanism occurs due to the glass transition phenomena, which results in a reversible change in viscosity [28]. The material transitions from the glassy to the sticky state, leading to the formation of agglomerates due to sintering [29,30].

1.1. Goals and contents

The use of a microwave sensor for inline moisture measurements during fluidized bed agglomeration processes is thoroughly examined in this study. The main objective of this study is to enable consistent and accurate monitoring of moisture during agglomeration at various operating conditions. It is intended to also showcase the effectiveness of the microwave sensor and analyze the effectiveness and trustworthiness of such a device, for real-time moisture monitoring within the fluidized bed, bringing up new opportunities for improved process control and optimization.

In this study the two following workflows are differentiated: calibration through (i) inline sampling, by drawing samples from the process chamber during the agglomeration process and analyzing the moisture content offline referred to as inline fluidized bed calibration (IFB) and (ii) the conditioned fixed bed calibration (CFB), which refers to conditioning of a settled particle bed using a climate chamber. In this work, the latter approach is applied to fast moving and dilute particle clusters in fluidized beds and then compared to the IFB calibration. During the CFB measurements particles are not moving (not fluidized) and in direct contact with the sensor, which allows for the whole sensor volume to be filled with particles, ensuring ideal conditions for measurements under different temperature and moisture conditions.

2. Material and methodology

2.1. Materials

For this study Maltodextrin, a complex carbohydrate obtained from

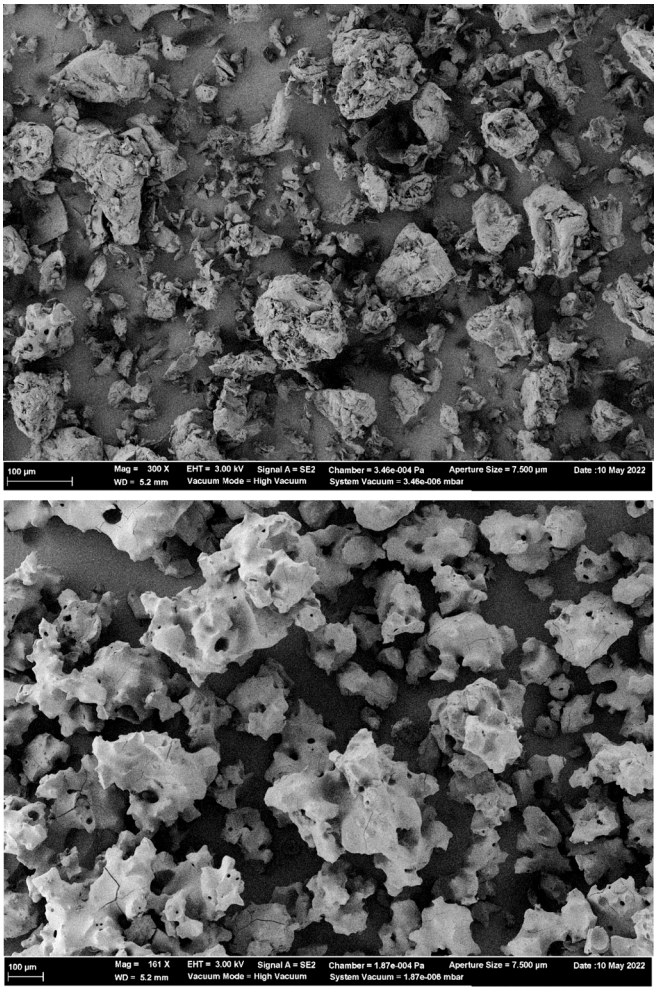

Fig. 2. Scanning electron microscopy image of MD20 before (top) and after (bottom) agglomeration in fluidized bed. There are visible structural differences on the particle surface at microscopic level.

the partial enzymatic breakdown of potato starch, is used. The selected form of maltodextrin has a dextrose content of around 20 wt%. The food grade maltodextrin Avebe MD20P (Biesterfeld AG, Germany) is used in this study.

Maltodextrin, as a polysaccharide, is composed of a series of glucose molecules connected by glycosidic linkages. The dextrose content, measured at 18.9 wt%, indicates the proportion of glucose present in the maltodextrin. The selection of this composition was due to its great solubility and functionality. Therefore, it is often used as model material in the food industry.

The material was kept in a controlled environment, considering temperature and humidity, to maintain its structural integrity until it was utilized in the experiments. In order to reduce product uncertainty, maltodextrin from a single producer and batch was used consistently throughout the trial.

2.2. Lab scale fluidized bed

The fluidized bed used in this study is the GF3 lab scale fluidized bed (Glatt GmbH, Germany). A scheme of the conical fluidized bed setup with internal filters is displayed in Fig. 1. The air distributor plate is 18 cm in diameter and has a mesh size of 105 µm. The fluidized bed is run in top spray configuration at a nozzle air pressure of 2 bar (absolute) and an air volume flow rate of 2 m^3/h. The nozzle setup consists of a Series 970-S4 (Düsen-Schlick GmbH, Germany) with a liquid nozzle orifice

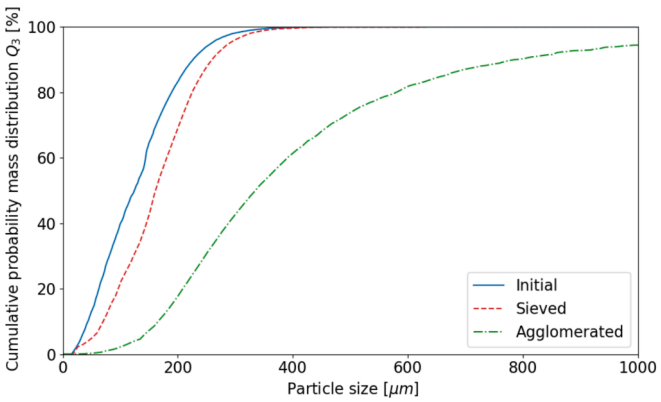

Fig. 3. Particle size distribution of the initial, sieved and final agglomerated material after the agglomeration experiment.

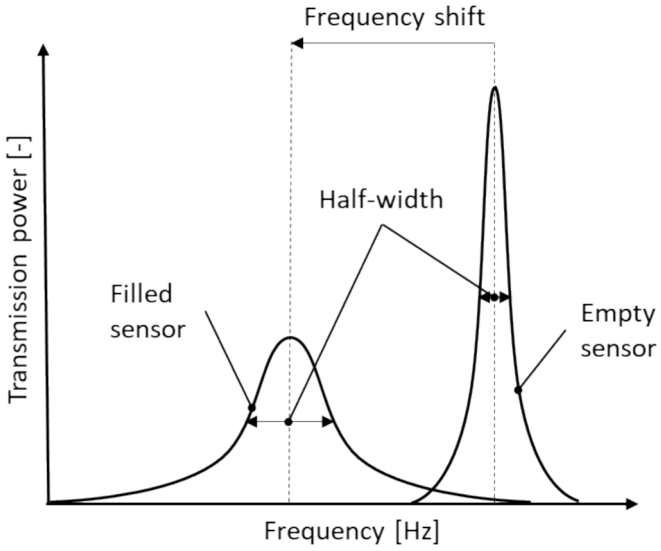

Fig. 4. Characterization of resonance curve with resonance frequency and the half width of resonance. Resonance curves of a filled and empty resonator volume.

diameter of 1.2 mm and the corresponding air cap at level 3 resulting in a spray angle of about 50°. The spray setting results in droplets with a $d_{50,3}$ of 33 µm. The exact spray characteristics can be found in [31] among others for different spray configurations. The spray nozzle is located 25 cm above the distributor plate. The liquid water is pumped into the chamber with a TBE peristaltic pump (MDX Biotechnik International GmbH, Germany). Experiments are performed in batch mode with a bed mass of 0.5 kg.

The microwave sensor is positioned at the lower process chamber port at a bed height of 6 cm. The sensor aligns with the process chamber wall and is therefore non-intrusive and suitable for agglomeration.

The filters are cleaned by reversing the flow direction through every single filter for 1 s at 5 bar (absolute). The process of filter cleaning is performed every minute and the cleaning cycle lasts for about 30 s, after which samples are collected. As a result, the sample drawing intervals are a multiple of the entire cleaning cycle, which lasts about 1.5 min in total. The samples for offline analysis are drawn from the sample drawer at a bed height of 16 cm and a radial depth of 2 cm.

In the sticky state, colliding particles form a viscous bridge that turns into a solid bridge upon drying due to sintering. The solid bridge eventually breaks due to stresses experienced through bed fluidization. The process results in coarse agglomerates starting from fine particles shown in Fig. 2 on the top and bottom respectively. The high-resolution scanning electron microscopy images are taken with a Supra 55 VP (Carl Zeiss AG, Germany).

The particle size of the powder has been determined using the dynamic image analyzer Camsizer XT (Microtrac Retsch GmbH, Germany). The maltodextrin powder is sieved before conducting agglomeration experiments as fine particles easily stick to filters and walls as a result of elutriation. After the agglomeration process, which takes a few minutes, substantial increases in particle size are detected, as shown in Fig. 3.

Furthermore, it is crucial to acknowledge that the porosity of the particles undergoes severe alteration during the process of agglomeration (data not shown). The probable cause of this is the creation of voids between the primary particles inside an agglomerate.

2.3. Microwave sensor

The microwave resonance technology exploits the interaction between water molecules and alternating electromagnetic fields. The frequency at which the sensor measures is determined in advance by the resonance wavelength of the microwave inducing resonator. When the resonator is filled with material, there is an increase in the storage of electric field energy, resulting in a decrease in the resonance frequency (Buschmüller et al., 2007). The microwave resonator method enables a moisture measurement that is independent of the sample mass. Alternatively, it is also possible to measure the mass of the product independently of its moisture content. The subsequent discussion will cover the fundamental principles of this measurement approach. A microwave resonator has multiple resonance frequencies, which correspond to certain frequencies at which microwave transmission reaches its maximum. The resonance frequencies are contingent upon the dimensions of the resonator. A resonance curve is defined by two parameters: (i) the resonance frequency and (ii) the width of the resonance curve at half of the maximum as shown in Fig. 4.

When a substance is introduced into the measuring volume of the sensor, it causes alterations in the properties of the resonance curve: (i) the resonance frequency decreases as the wavelength within the material decreases and (ii) the resonance curve widens because of microwave energy losses within the material [17].

As the moisture content increases, the resonance curve shifts towards lower frequencies and the amplitude at resonance diminishes (Knöchel et al., 2001).

Thus, the measured quantities consist of the shift of the resonance frequency and the augmentation of the half-width of the resonance curve. Therefore, by measuring two factors, namely the moisture content and the mass of the product being measured, it is possible to determine both unknown material properties. Since the changes in the resonance curve are identified in every measurement, the empty state of the resonator also holds significance for the measurement. Hence, it is necessary to determine the parameters of the resonance curve of the empty resonator. Defining this empty state at the expected process temperature prior to each measurement is highly recommended. The determination of the measurement signal is as follows:

The first parameter to determine is the change in the resonance frequency A with f_0 the resonance frequency of the empty and f_f of the filled sensor in Hz [17]:

$$A = f_0 - f_f \tag{1}$$

The second parameter is the increase of the half-width B with w_0 the half-width of the resonance curve of the empty and w_f half-width of the resonance curve of the filled sensor [17]:

$$B = w_f - w_0 \tag{2}$$

Combining the two parameters allows the calculation of the mass-independent microwave moisture S:

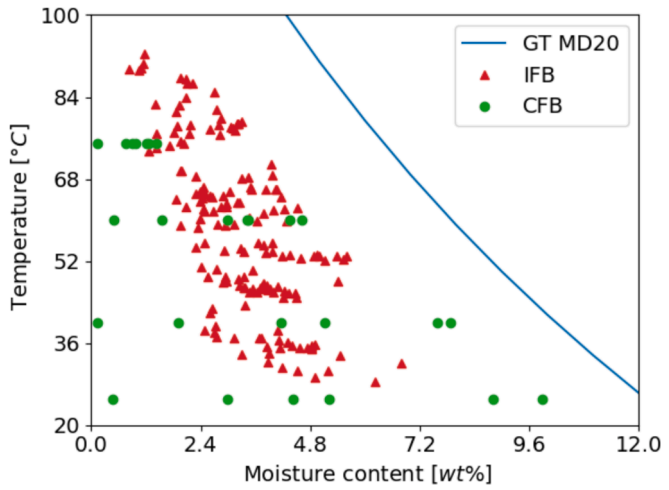

Fig. 5. The investigated moisture content and temperature range compared to the glass transition temperature of the used material MD20 (GT MD20). The model to determine the glass transition as a function of moisture content is from Gordon and Taylor [35] and is shown in Equation (11). The figure also contains the IFB and CFB samples.

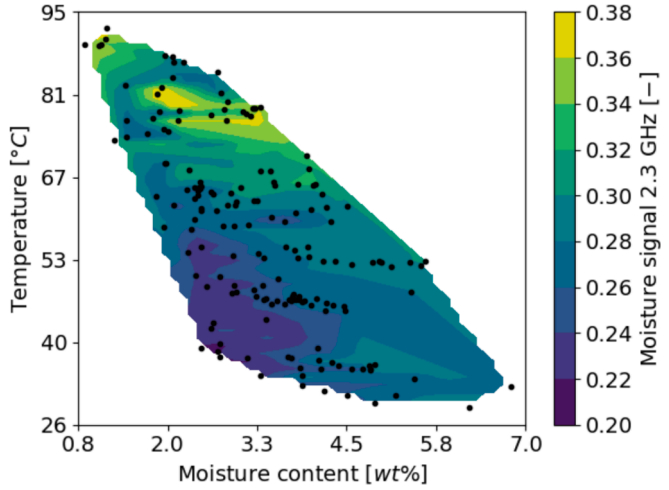

Fig. 6. Interpolated surface of the MW moisture signal at 2.3 GHz of MD20 for a moisture content and temperature range. The black dots show the moisture content and temperature of the IFB samples.

$$S = arctan\left(\frac{B}{A}\right) \tag{3}$$

Both parameters A and B exhibit the same mass-dependent relationship. Hence, the division of A by B is mass independent. In theory the outcome is solely determined by the measured moisture content of the material. The arc tangent of this quotient is computed to constrain the range of the moisture value between 0 and 1 as a dimensionless value [17].

The granule moisture content is measured using the MW 4200 (TEWS Elektronik GmbH & Co. KG, Germany) microwave resonance sensor. The sensor allows to use two frequencies 2.3 GHz and 5.6 GHz simultaneously. This measurement is influenced by the particle position. Particles near or in direct contact with the sensor show agreement while with increasing distance from the sensor the microwave signal increases and fluctuates more. The experimental evaluation of the impact of the particle position in the measurement volume is shown in the appendix.

It is confirmed that the device can determine the moisture content independent of the mass, which is a function of bulk density due to a constant measurement volume as shown in appendix. This makes it suitable for agglomeration processes with bulk density changes.

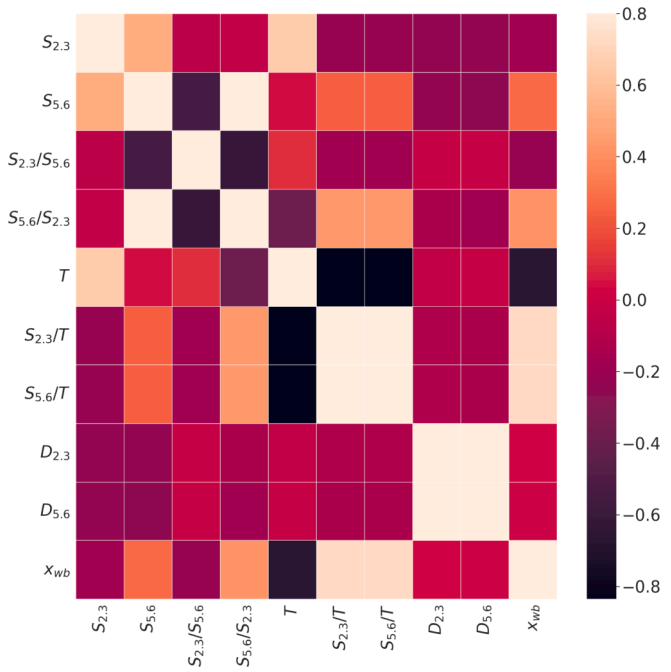

Fig. 7. The Pearson coefficient as a heat map.

2.4. Conditioned fixed bed sample preparation

To compare the prediction of the calibration a second approach, using a CFB, is chosen. This allows to create a controlled environment and eliminate all phenomena that occur naturally in a fluidized bed that may have a negative impact on the measurements, such as bubble formation, channeling near the wall, material sticking to the sensor and determination of the particle temperature. The material is conditioned for over a week at different moisture contents and temperatures using the climate chamber ICH 110 (Memmert GmbH+Co. KG, Germany). The examined sample volume is chosen to be a multiple of the previously determined measurement depth and sensor width to ensure the entire sensor measurement volume is filled with material. The CFB samples are supposed to cover the same moisture content and temperature range as the IFB samples. The conditioned sample values are displayed in Fig. 5.

The conditioning of the material in a climate chamber is done by setting the relative humidity and temperature. With these parameters, it is possible to determine the resulting equilibrium moisture content of the material using the sorption isotherm displayed in Fig. 16 shown in the appendix.

2.5. Feature selection

The surface plot of the microwave moisture signal at 2.3 GHz in Fig. 6 shows that at low temperatures and low moisture content the signal is also low. The signal appears to increase not only with increasing moisture content but also with increasing temperature. Deriving a model to predict the moisture content when looking at the correlation between the signals and the moisture content of the samples appears difficult as multiple parameters affect the signal of the sensor. Therefore, feature selection is applied to identify the relevant input parameters to get the best prediction. Surface plots as shown in Fig. 6, in addition to Figs. 21-23 in the appendix, visualize the correlation between the input and target values.

Feature selection is applied, as it is common in machine learning, to find appropriate input parameters that show a high correlation to the target value. In order to reduce the number of input parameters of the

Table 1
Process parameters used in lab-scale batch agglomeration experiments.

Inlet air flow rate [m^3/h]	Inlet air temperature [°C]	Spray rate [g/min]
60	40	6
75	60	10
80	70	12
85	80	14
100	100	18

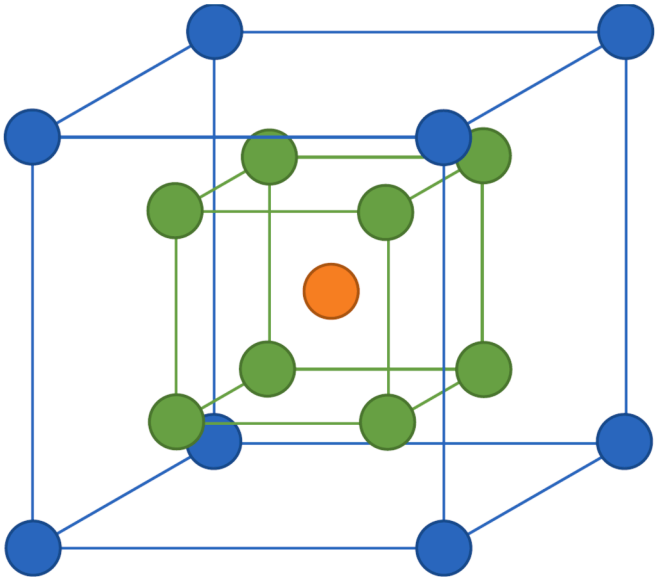

Fig. 8. Experimental design matrix.

Table 2
Coefficients and threshold of IFB calibration.

C_1	C_2	C_3	C_4	$S_{Threshold}$
−163.14	110.37	−10.72	−0.07	0.33

model it is important to identify dependencies of the input parameters among each other [32,33].

Two distinct criteria are utilized to characterize the degree of correlation between the input parameters and the target and the input parameters with each other. The first parameter, the Pearson correlation coefficient, characterizes the linear relationship between two populations Z and Y:

$$\rho_{Z,Y} = \frac{Cov(Z,Y)}{\sigma_Z \sigma_Y} \tag{4}$$

The standard deviations of each population are denoted by σ_Z and σ_Y. The Spearman rank correlation coefficient is selected as the second parameter to quantify non-linear correlations. In order to evaluate the relationship between the input parameter and the target it can be characterized using a monotonic function:

$$r_{Z,Y} = \frac{Cov(r_{g,Z}, r_{g,Y})}{\sigma_{r_{g,Z}} \sigma_{r_{g,Y}}} \tag{5}$$

The ranks of a quantity are $r_{g,Z}$ and $r_{g,Y}$, the smallest value having rank 1. The standard deviations of each ranking are $\sigma_{r_{g,Z}}$ and $\sigma_{r_{g,Y}}$.

The selection of input parameters is done by comparing the Pearson coefficient and Spearman coefficient. An overview is given by the heatmap in Fig. 7 visualizing the Pearson coefficient of the input parameters and the target value as well as the input parameters among each other. The heatmap for the Spearman coefficient and histograms can be found in the appendix. In Table 5 the Pearson coefficient and Spearman rank coefficient of the input parameters with the target value is displayed.

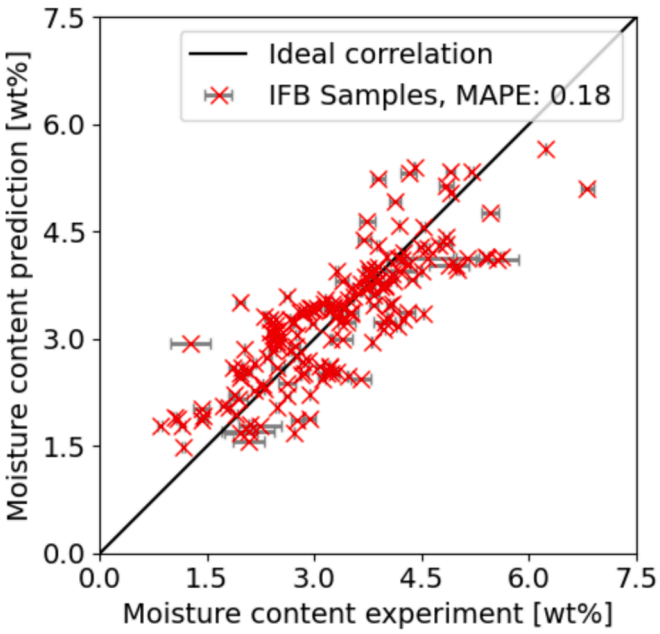

Fig. 9. Parity plot showing the predicted moisture content using IFB calibration over the IFB samples. The predictions are made using Eq. (6). The MAPE equals 18% and the relative accuracy is 82%.

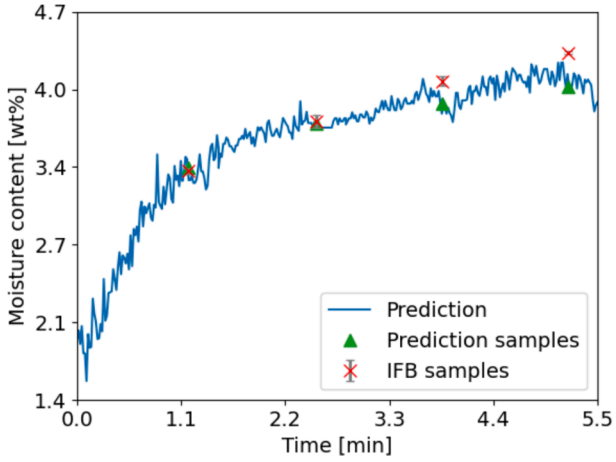

Fig. 10. Moisture content evolution over time during fluidized bed agglomeration experiment 23.

The input parameters are the four signals retrieved from the microwave sensor ($S_{2.3}$, $S_{5.6}$, $D_{2.3}$, $D_{5.6}$) and the temperature T. Additionally, various combinations are investigated such as the quotient of microwave moisture content signal and the temperature ($S_{2.3}/T$, $S_{5.6}/T$) and the quotient of the microwave moisture at different frequencies ($S_{2.3}/S_{5.6}$, $S_{5.6}/S_{2.3}$). The quotient of microwave moisture content signal and the temperature ($S_{2.3}/T$, $S_{5.6}/T$) represents a decreasing moisture content in case of a decrease in moisture content signal or in case of an increase in temperature. The quotient of the microwave moisture at different frequencies ($S_{2.3}/S_{5.6}$, $S_{5.6}/S_{2.3}$) is added to cover a larger range of moisture content with multiple frequencies. The temperature T has a high negative correlation to the target value and the highest correlation of individual signals overall. The quotients of the microwave moisture signal and the temperature ($S_{2.3}/T$, $S_{5.6}/T$) has the highest correlation of all

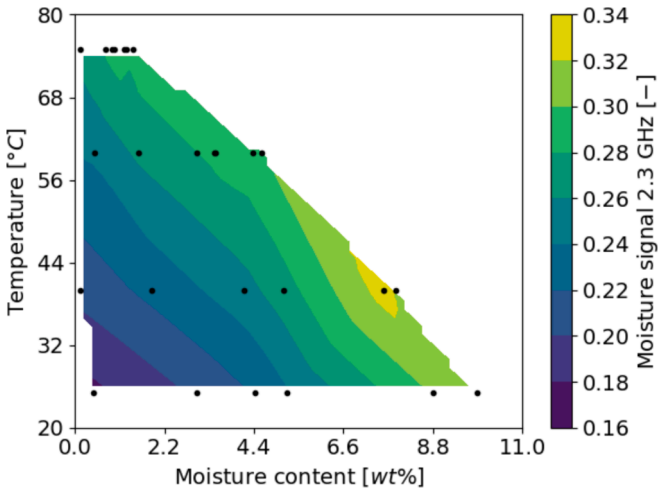

Fig. 11. Interpolated contour of the MW moisture signal at 2.3 GHz of MD20 for a pre-set moisture content and temperature range. The black dots show the moisture content and temperature of the CFB samples.

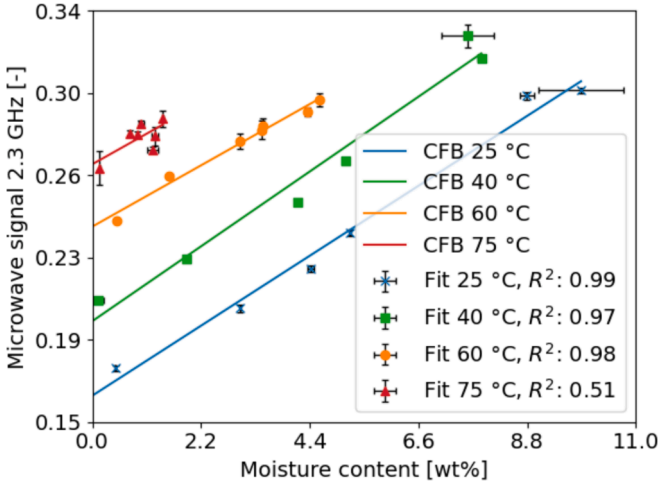

Fig. 12. MW moisture signal at 2.3 GHz of MD20 plotted over the CFB calibration samples at different temperatures.

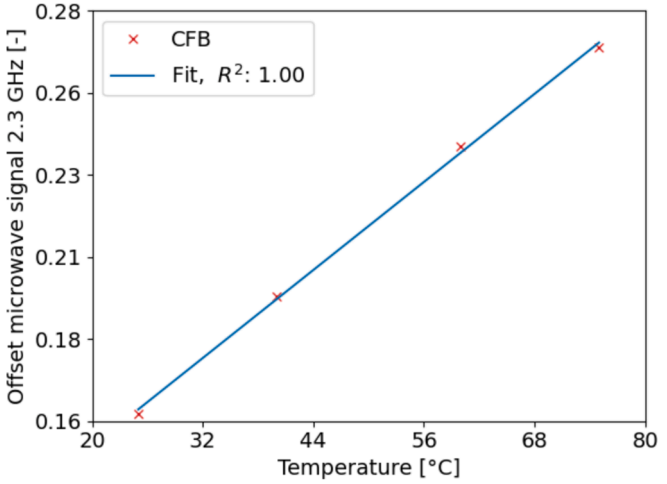

Fig. 13. Moisture signal function offset plotted over the temperature.

Table 3
Coefficients of CFB calibration equation.

C_1	C_2	C_3
0.0140	0.0021	0.1098

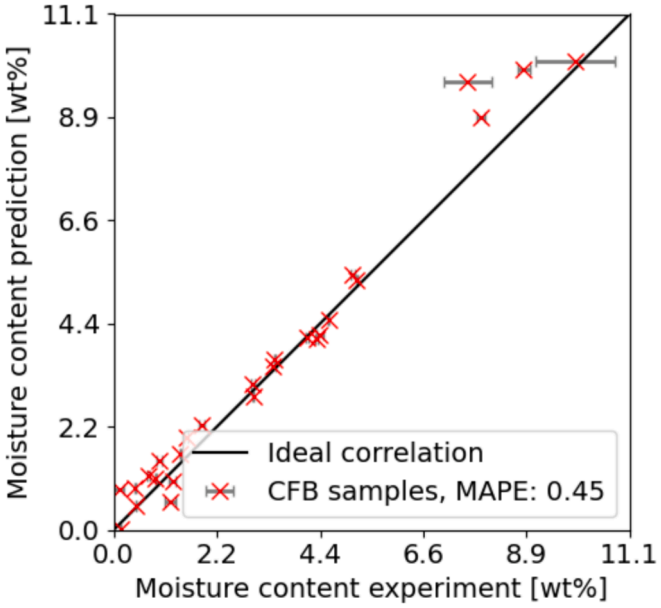

Fig. 14. Parity plot showing the predicted moisture content using CFB calibration over the CFB samples. The predictions are made using Eq. (10).

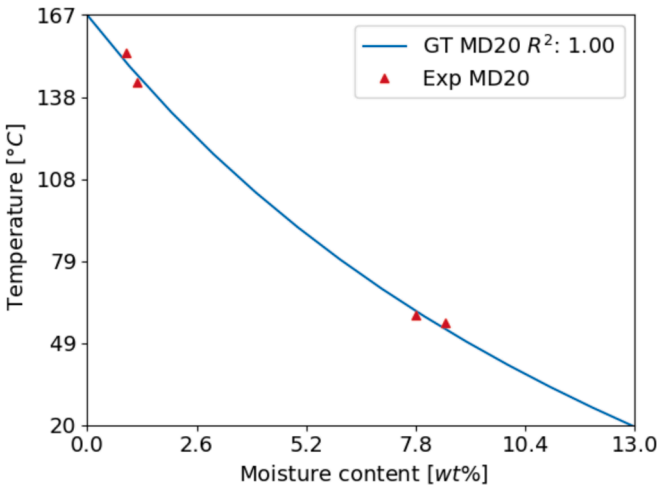

Fig. 15. Glass transition temperature of MD20 over increasing moisture content. GT refers to the Gordon and Taylor equation [35]. The equation fits with an R^2 of 1.00 using parameter k of 6.4.

input parameters. The temperature and the quotients of the microwave moisture signals and the temperature ($S_{2.3}/T$, $S_{5.6}/T$) have a similar high correlation to the target and a very high correlation with the temperature T. Therefore, the quotients of the microwave moisture signals and the temperature ($S_{2.3}/T$, $S_{5.6}/T$) are discarded and the temperature T is chosen as the first input parameter.

The quotient of the microwave moisture signals ($S_{2.3}/S_{5.6}$, $S_{5.6}/S_{2.3}$) and the microwave moisture signal at 5.6 GHz $S_{5.6}$ have a higher nonlinear correlation than the microwave moisture signal at 2.3 GHz $S_{2.3}$ but are at a similar level when it comes to linear correlation. The microwave moisture signal at 5.6 GHz $S_{5.6}$ has a very high standard

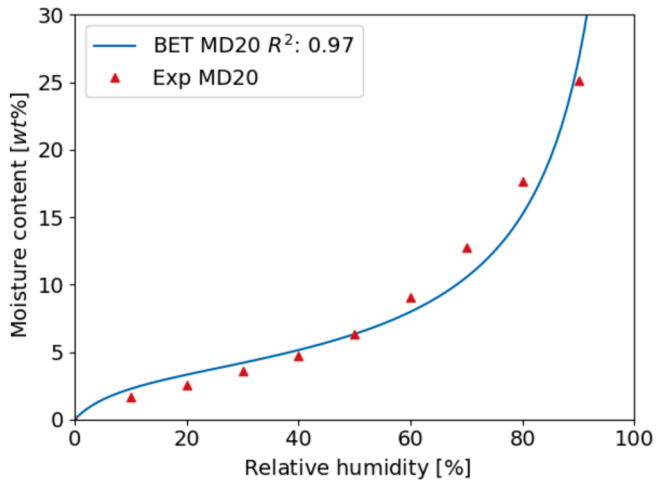

Fig. 16. Adsorption isotherm of MD20 at 20 °C. BET refers to the Brunauer–Emmett–Teller equation [36]. The model fits with an R^2 of 0.97 using parameters *mm* and *n* with values of 3.7 and 11.9 respectively at 20 °C.

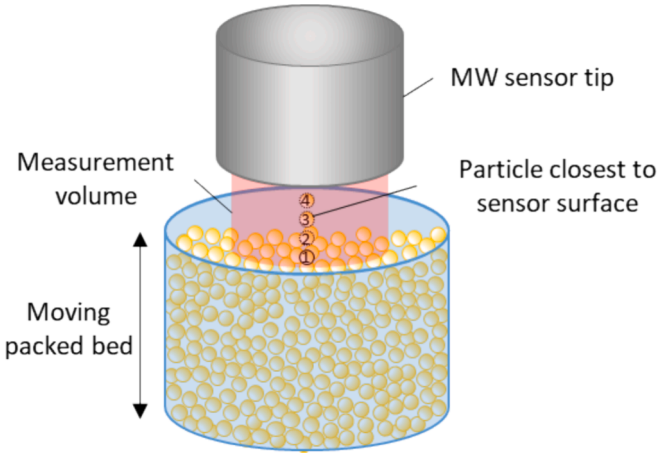

Fig. 17. Experimental setup to investigate impact of particle position and MW measurement volume filling level by approaching the sensor with a packed bed perpendicular to the sensor surface.

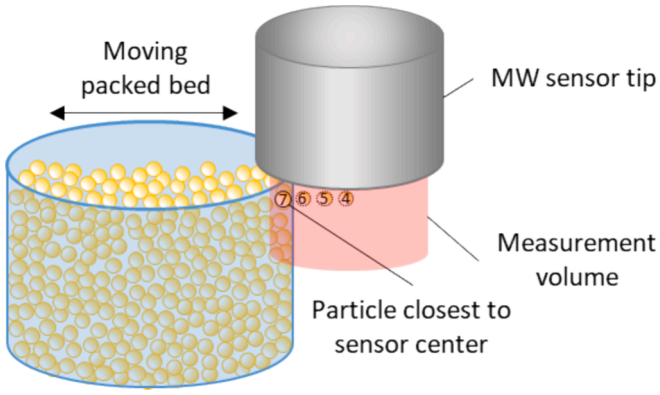

Fig. 18. Experimental setup to investigate impact of particle position by approaching the sensor with a packed bed perpendicular to the sensor axis, while maintaining contact with the sensor surface.

deviation of about 10 % while the microwave moisture signal at 2.3 GHz $S_{2.3}$ has a lower standard deviation and enables therefore a better error propagation. The microwave density signals ($D_{2.3}$, $D_{5.6}$) have a very low linear correlation to the target and are therefore not considered. Therefore, the microwave moisture signal at 2.3 GHz $S_{2.3}$ is chosen as a second input parameter. This final set of input parameters allows to differentiate the impact of moisture and temperature.

2.6. Design of experiment

The process parameters modified during the experiments are the fluidization volume air flow rate, the inlet air temperature and the liquid spray rate as displayed in Table 1.

Given the complexity of the operation, the limit process conditions, at which agglomeration is still possible, need to be outlined in order to build the DoE. In order to conduct the experimental study, a two-phase full factorial design was selected, which led to the creation of an extended full factorial design that includes a center point [34].

Each parameter was assigned an upper and a lower limit. Furthermore, the average value of these limits was used as the third level to identify non-linear patterns. Two additional levels, the fourth and fifth, are introduced between the lower and upper bounds and the average value to facilitate the estimation of quadratic terms in models. This would result in a total of 125 experiments in the five-level full factorial approach, therefore a two-phase strategy is chosen. The experimental design space is visualized in Fig. 8. This design results in a total of 17 individual experiments. Experiments are ended when defluidization occurred or the equilibrium moisture content is reached.

The number of experiments needed for calibration can be reduced to a minimum. Samples and experiments needed to be removed from the dataset due to defluidization ultimately leading to an inhomogeneous moisture distribution and inconsistent measurements. The removal of samples and experiments is executed in case of high standard deviation due to measurement errors or too fast agglomeration leading to heterogeneously distributed bed. The final dataset comprises 29 experiments and 169 samples.

3. Results and discussion

In the following chapters the application of the two calibration workflows in fluidized beds is discussed. Typically, the CFB calibration is preferred since ideal conditions for calibration can be established.

3.1. Inline fluidized bed calibration

With the identified input parameters $S_{2.3}$ and T from section 2.5 it is possible to build a model using multivariable regression. The results are compared and discussed.

The calibration uses the 2.3 GHz moisture signal of the microwave sensor. The input parameters are used in a second order approach: $S_{2.3}$ refers to the signal at 2.3 GHz, T to the temperature, x_{wb} is the predicted wet based moisture content in wt%. C_1, C_2, C_3 and C_4 are fitting coefficients and S_{Thresh} is a threshold that equals the maximum of the second order polynomial:

$$x_{wb}(S_{2.3}, T) = \begin{cases} max\left(0, C_1 S_{2.3}^2 + C_2 S_{2.3} + C_3 + C_4 T\right), S_{23} < S_{Threshold} \\ C_1 {S_{Threshold}}^2 + C_2 S_{Threshold} + C_3 + C_4 T, S_{23} \geq S_{Threshold} \end{cases} \quad (6)$$

For the regression Excel Solver GRG Nonlinear is used. The fit is achieved by minimizing the sum of the squared error. This leads to parameters C_1, C_2, C_3 and C_4 as shown in Table 2.

The equation fits the total dataset with a MAPE of 0.18. The fit is visualized in a parity plot in Fig. 9. The points are distributed around the ideal correlation at 45° with an almost constant offset. The relative deviation at lower moisture contents is higher than at higher moisture contents.

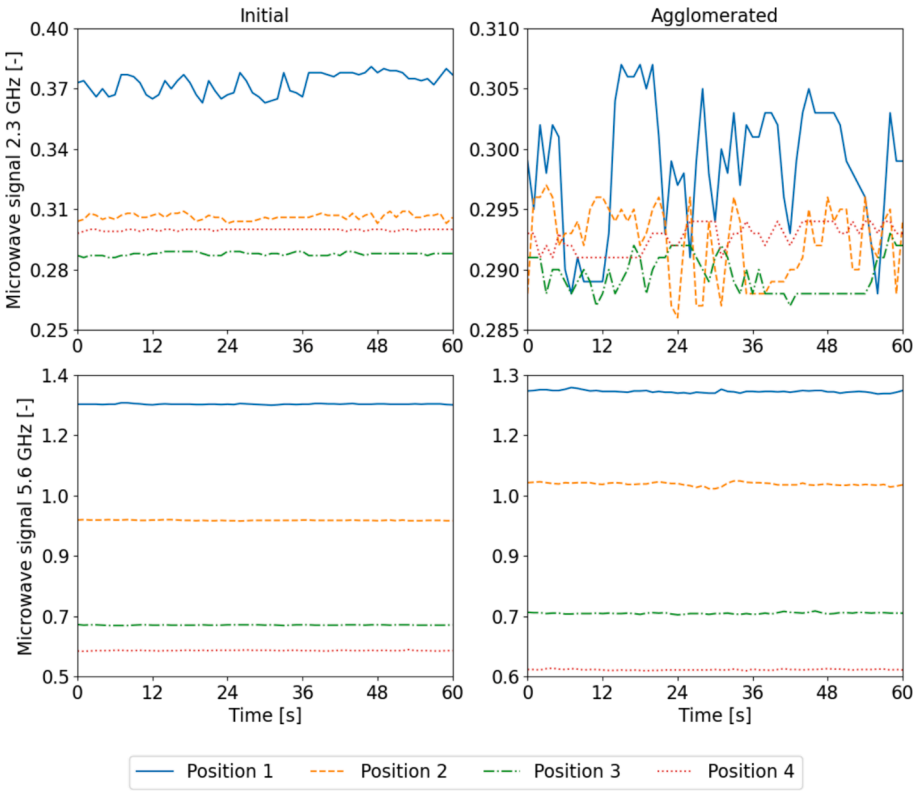

Fig. 19. Microwave signal evolution over one minute at 2.3 and 5.6 GHz for initial (left) and agglomerated (right) material. The positions correspond to Fig. 17 where position 4 is in contact with the sensor and 1 is the farthest away.

It indicates that there are experiments with a very poor prediction, while the majority has a good prediction quality. The error increases with increasing inlet air temperature and decreasing water spray flow rate, which results in lower moisture contents and higher temperatures.

An example plot of the moisture progressing over time showing experiment 23 is shown in Fig. 10. The predicted moisture content over time is plotted against the IFB samples.

3.2. Conditioned fixed bed calibration

The contour plot in Fig. 11 shows that the microwave moisture signal at 2.3 GHz not only increases with the moisture content but also with the temperature. The authors would have expected an increase of the microwave moisture signal only with increase of the moisture content of the particles. When looking at Fig. 12 clear trends are visible, which allows to derive a model based on the trends instead of using feature selection.

The figures for the surface plot of the MW moisture content signal 5.6 GHz, MW density signal 2.3 GHz and MW density signal 5.6 GHz can be found in the appendix.

In Fig. 12 the MW moisture content signal at 2.3 GHz shows a linear correlation to the moisture content. The linear fit is very high but decreases with increasing temperature. Additionally, the slopes are similar at different temperatures while they maintain different offsets. The figures for MW moisture content signal at 5.6 GHz, MW density signal at 2.3 GHz and 5.6 GHz are shown in the appendix as they do not show clear patterns and correlations to the moisture content.

This linear dependency allows to assume that the slope is solely correlating to the MW moisture content signal at 2.3 GHz while the temperature only correlates to the offset. In Fig. 12 also a systematic offset at different temperatures can be seen:

$$S_{2.3} = C_1 x_{wb} + f(T) \tag{7}$$

Equation (7) can be reformulated for the moisture content as follows, where C_1 is the average slope:

$$x_{wb} = \frac{S_{2.3} - f(T)}{C_1} \tag{8}$$

The offset is a function of the temperature as shown in Fig. 12. In Fig. 13 the offset is plotted against the temperature and it can be seen that the offset is a linear function of the temperature.

The offset is a linear function of the temperature with a R^2 of 1.00:

$$Offset = C_2 T + C_1 \tag{9}$$

With the newly found correlation and dependencies of moisture content on MW moisture content signal at 2.3 GHz and temperature it is possible to derive an equation for calibration by combining Equation (8) and Equation (9). Starting with the linear dependency of the moisture content on the MW moisture content signal at 2.3 GHz leading to Equation (10). S_{23} refers to the microwave moisture signal at 2.3 GHz and T refers to the particle temperature:

$$x_{wb} = \frac{S_{2.3} - C_2{}^{*}T + C_3}{C_1} \tag{10}$$

The coefficients C_1, C_2 and C_3 stem from the average slope in Fig. 12 and the temperature dependency in Fig. 13, resulting in Equation (10) with the parameters C_1, C_2 and C_3 as summarized in Table 3.

The parity plot in Fig. 14 shows that a great fit with a MAPE of 0.45 and R^2 of 0.96 is achieved and the model is able to accurately predict the moisture content.

When applying the IFB calibration derived in section 3.1 a MAPE of 194 % is reached, Fig. 25. This shows that the IFB calibration is only applicable to fluidized beds. The prediction above a moisture content of 3 wt% is overestimated, while in the lower moisture content range it is underestimated.

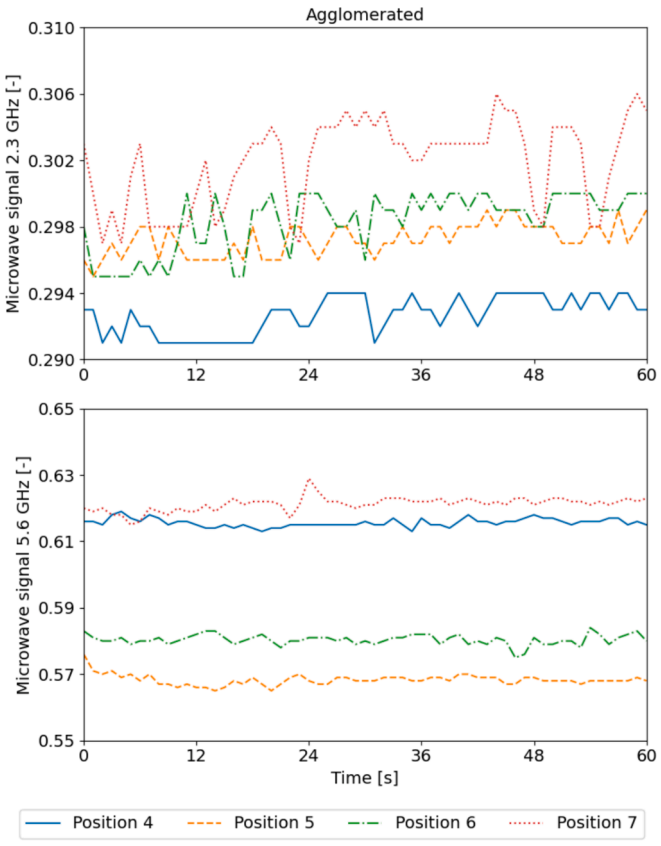

Fig. 20. Microwave signal evolution over one minute at 2.3 and 5.6 GHz for agglomerated material. The positions correspond to Fig. 18 where position 4 is the sensor center and 7 is the farthest away from the center.

Table 4
Process parameters of fluidized bed experiments.

Experiment	Air flow rate [m^3/h]	Temperature [°C]	Water flow rate [g/min]
1	80	70	12
2	80	70	12
3	60	40	6
4	100	100	6
5	60	100	18
6	100	40	6
7	60	100	6
8	100	40	18
9	100	100	18
10	75	60	10
11	75	80	10
12	75	80	14
13	85	60	10
14	85	80	10
15	85	80	14
16	80	70	12
17	60	40	6
18	100	100	6
19	100	40	6
20	60	100	6
21	100	100	18
22	75	60	10
23	75	60	14
24	75	80	10
25	75	80	14
26	85	60	10
27	85	60	14
28	85	80	10
29	85	80	14

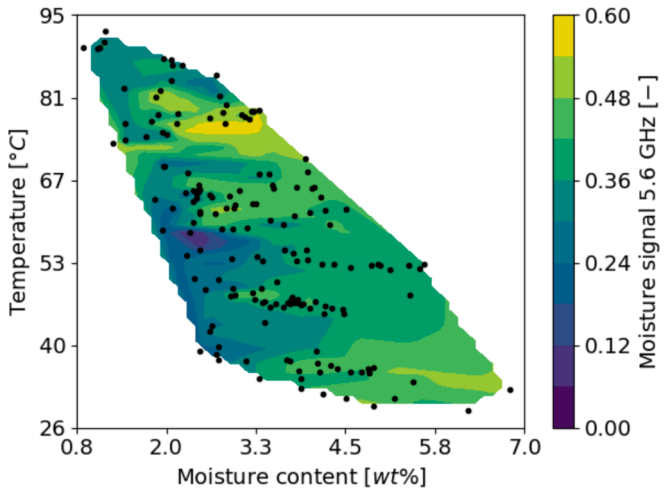

Fig. 21. Interpolated contour of the MW moisture signal at 5.6 GHz of MD20 for a moisture content and temperature range. The black dots show the moisture content and temperature of the IFB samples.

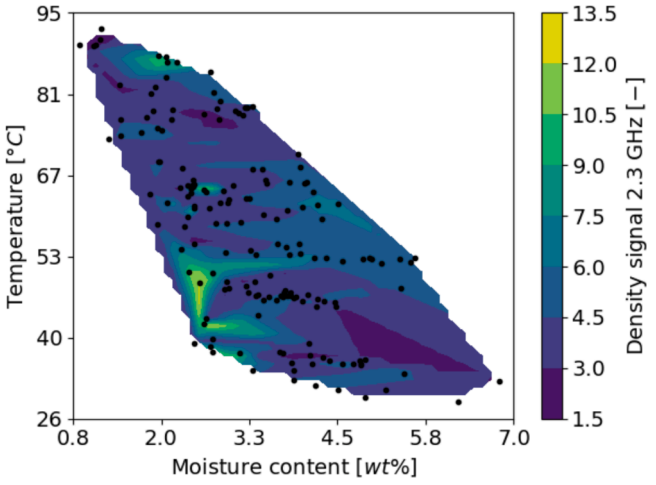

Fig. 22. Interpolated contour of the MW density signal at 2.3 GHz of MD20 for a moisture content and temperature range. The black dots show the moisture content and temperature of the IFB samples.

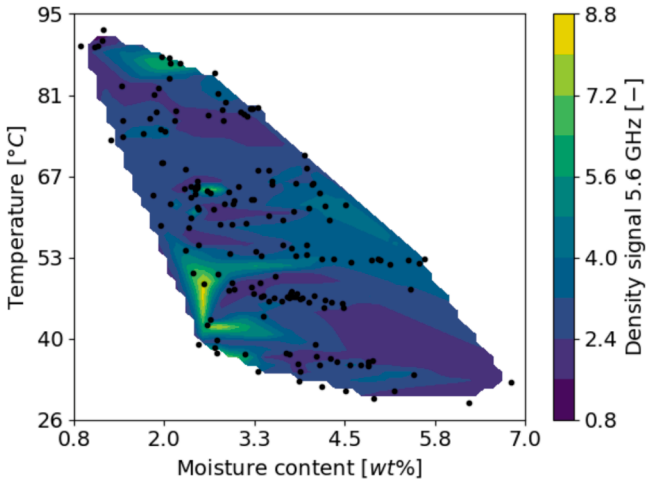

Fig. 23. Interpolated contour of the MW density signal at 5.6 GHz of MD20 for a moisture content and temperature range. The black dots show the moisture content and temperature of the IFB samples.

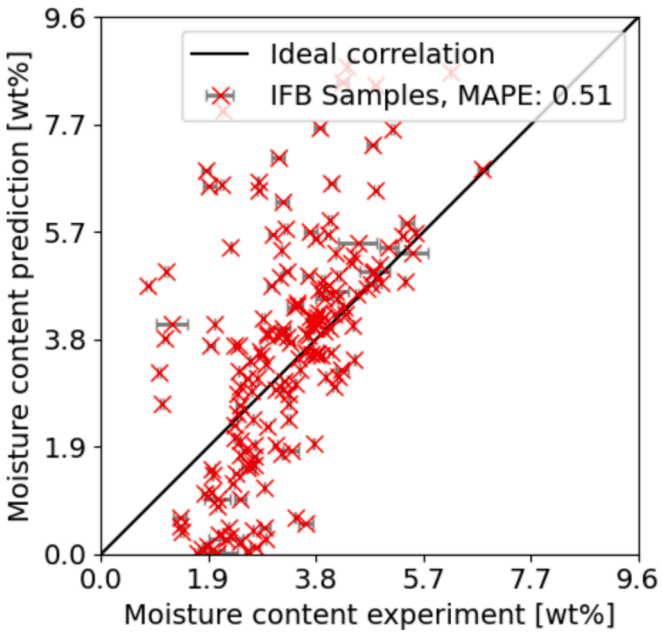

Fig. 24. Parity plot showing the predicted moisture content using CFB calibration over the IFB samples. The MAPE is 49%.

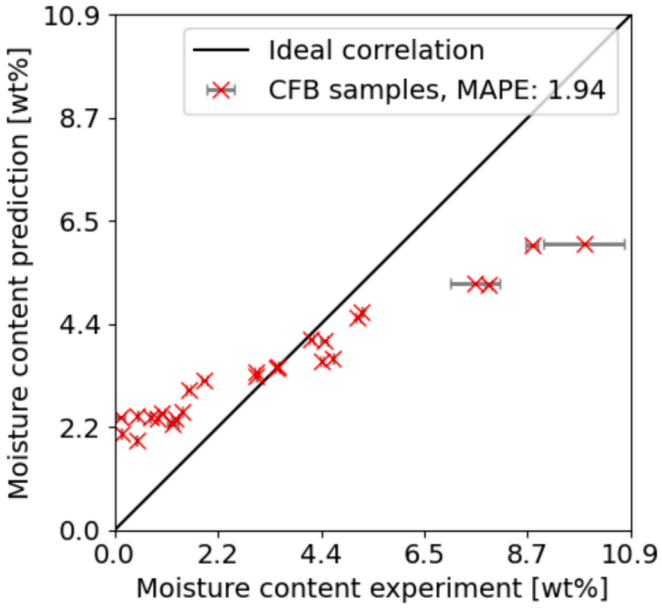

Fig. 25. Parity plot showing the predicted moisture content using IFB calibration over the CFB samples.

When investigating the 5.6 GHz signal a clear pattern cannot be found. This might be due to the reason that higher frequencies are usually applied to higher moisture contents, which are seldom reached in the current experimental set-up and thus, resulting in unreliable values.

When applying the CFB calibration to the IFB data from 3.2 it results in a MAPE of 51 %. As the parity plot in Fig. 24 shows, the prediction quality is poor. This shows it is only possible to derive a mechanistic approach from CFB measurements that is valid for fixed beds.

These results show that the two different experimental cases need different calibration workflows. The CFB calibration does not capture the same behavior as the IFB calibration. This might be due to the (i) lower number of CFB samples and a result of overfitting, the (ii) fluctuations in the fluidized bed influencing the measurement due to bubbles moving between the sensor tip and material or due to the way of (iii) recording the particle temperature.

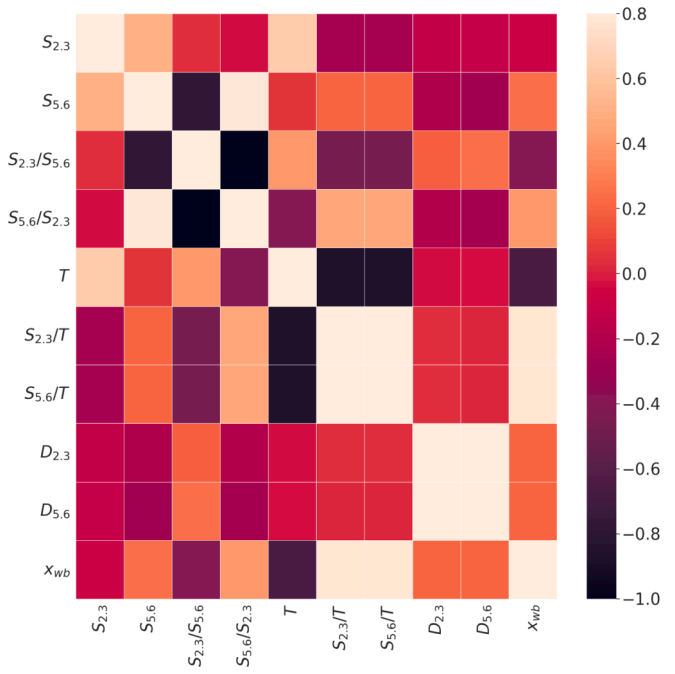

Fig. 26. The Spearman coefficient as a heat map.

The impact of the distance between material and the sensor on the measurement is severe as shown in the appendix. Above a certain threshold the increasing distance leads to an increase of the microwave signal and the signal fluctuates more. Bubble and void formation in fluidized beds is natural. Considering the effects of the distance, the impact of bubbles on the measurement is severe, therefore the positioning of the sensor is essential. The authors recommend placing the sensor in a position where the material is very close to the wall or sensor and does not form voids such as the annular zone in a spouted bed, a downer in a circulating fluidized bed or connecting pipes between process units. In case of inline measurements in a fluidized bed, as it is examined in this study, it is recommended to add a recycle stream from and to the process chamber and to measure in the pipes or letting the material settle on the sensor before reintroduction. In case direct measurement in the chamber is preferred it is recommended to position the sensor as low as possible to ensure the sensor is covered in material.

The authors suggest using the (i) IFB workflow for inline measurements in fluidized beds or processes forming bubbles or any type of voids and the (ii) CFB workflow for online measurements for fixed beds or dense particle clusters. It is recommended to preheat the sensor outside of device and set the empty reference state before the experiment, so all have the same reference point. This allows to account better for temperature influences for a large range of process parameters and the resulting process conditions.

Accuracy of the calibration can be improved by reducing the predictive range of the calibration. It is still possible to achieve high accuracy, R^2 of 0.9 and above, when the calibration is done for a single experiment. This agrees with what has already been done in literature [17,19,21,20].

Comparing the two workflows regarding time effort shows that the IFB calibration is faster to execute (within weeks), while the CFB approach takes multiple weeks and up to several months due to the long duration of conditioning of the material. The IFB calibration also requires access to a fluidized bed and size, while the CFB calibration only requires a climate chamber for conditioning.

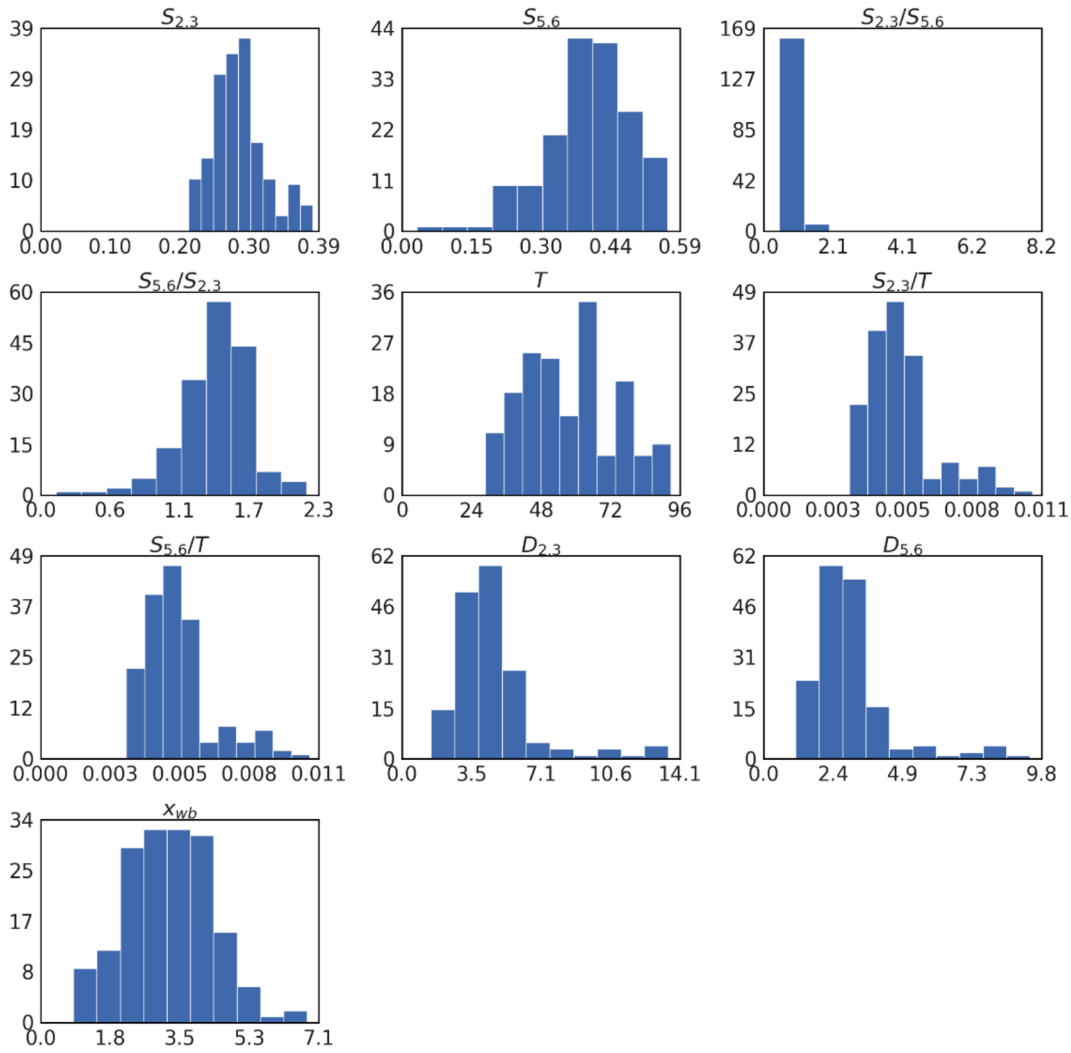

Fig. 27. The input parameters displayed as histogram.

Table 5
Pearson and Spearman coefficients of the input parameters to the target values of the IFB data.

Input parameter	Pearson coefficient	Spearman coefficient
$S_{2.3}$	−0.17	−0.09
$S_{5.6}$	0.28	0.25
$S_{2.3}/S_{5.6}$	−0.21	−0.40
$S_{5.6}/S_{2.3}$	0.43	0.40
T	−0.68	−0.67
$S_{2.3}/T$	0.73	0.77
$S_{5.6}/T$	0.73	0.77
$D_{2.3}$	0.02	0.21
$D_{5.6}$	0.01	0.20

4. Conclusion

In this study two workflows (inline fluidized bed and conditioned fixed bed) for the calibration of a two-resonance frequency microwave sensor are developed and compared. The derived calibrations are valid for a wide moisture content and temperature range and can be applied to dense or dilute particle clusters. The results of the study have shown that there are two types of calibration necessary for dense and dilute particle clusters.

Using a statistical experimental strategy, fluidized bed agglomeration experiments were conducted with various combinations of process parameters to examine the capabilities of the microwave sensor at different process conditions. The true moisture content is determined with the gravimetric method. To find the best input parameter set for the calibration feature selection is used.

As a second approach a fixed bed is examined under ideal conditions. The material is conditioned in a climate chamber. From these measurements a linear correlation describing the temperature dependency of the microwave signal was found.

The impact of bubbles in the fluidized bed on the microwave measurement is simulated by placing the materials in different positions of the measurement volume. The microwave signal shows a high dependency on the particle position. This is expressed by an increase in the signal with increasing distance from the sensor as well as an increasing fluctuating signal. Further it was found that for this type of material, range of moisture and temperature one frequency achieves a higher accuracy than two frequencies combined.

In summary, a major development in the field of process monitoring has been made with the use of multi-resonance microwave sensors for in-line moisture monitoring of fluidized bed agglomeration. A few benefits of this innovative technology are increased precision, improved process control and real-time, non-invasive measurement capabilities. It is clear from the thorough analysis of current research and case studies that this strategy has a lot of potential for streamlining fluidized bed agglomeration operations in a variety of industrial settings.

The utilization of multi-resonance microwave sensors in fluidized

bed agglomeration process monitoring presents a viable approach to enhance process effectiveness, minimize operational expenses, and elevate product quality. This technology has the potential to significantly impact several sectors and increase process control and monitoring with further study and development.

CRediT authorship contribution statement

Gero Stoeckl: Writing – review & editing, Writing – original draft, Visualization, Validation, Methodology, Investigation, Formal analysis, Data curation, Conceptualization. **Aitor Atxutegi:** Writing – review & editing, Supervision, Methodology, Investigation, Conceptualization. **Stefan Bellinghausen:** Writing – review & editing, Visualization, Supervision, Resources, Project administration, Funding acquisition. **Stefan Heinrich:** Writing – review & editing, Visualization, Supervision, Resources, Project administration, Funding acquisition.

Declaration of competing interest

The authors declare that they have no known competing financial interests or personal relationships that could have appeared to influence the work reported in this paper.

Acknowledgements

This project has received funding from the European Union's Horizon 2020 research and innovation programme under the Marie Skłodowska Curie grant agreement No 955661.

The authors would like to thank Zhi Cheng Hua, doctoral researcher at Hamburg University of Technology, for the technical assistance during the experiments on the lab scale device. The authors would like to thank Teresa Kurtz, doctoral researcher at Hamburg University of Technology, for the technical assistance. The authors would like to thank Marie Schellenberg, student at Hamburg University of Technology, for the contributions during the experiments on the lab scale device.

Appendix

Material

The measured poured bulk density of the powder is 564 kg/m^3. After grinding the material to a fine powder, the helium pycnometer AccuPyc 1330 (Micromeritics Instrument Corporation, United States) is employed to measure its skeletal density of 1480 kg/m^3. The moisture level of the powder remains continuously at around 3 wt% during storage.

In the fluidized bed liquid water is fed through the top spray into the process chamber. The liquid is atomized by the pressure of the air in the two-fluid nozzle. The glass transition temperature of the maltodextrin was measured at different moisture contents using a differential scanning calorimeter DSC 204F1 Phoenix (NETZSCH-Gerätebau GmbH, Germany). The discrete data points are fit using the Gordon and Taylor equation [35] shown in Equation (11). The equation describes the glass transition temperature as a function of the glass transition temperature of the pure components $T_{g,w}$ and $T_{g,s}$, the mass fraction of liquid x_{wb} and a fitting constant k:

$$T_g = \frac{k x_{wb} T_{g,w} + (1 - x_{wb}) T_{g,s}}{k x_{wb} + (1 - x_{wb})} \tag{11}$$

The glass transition temperature of the solid material $T_{g,s}$ equals 167 °C and of water $T_{g,w}$ is −135 °C. The resulting curve is displayed in Fig. 15.

The material is conditioned using a climate chamber for the CFB calibration. The correlation between temperature relative humidity and granule moisture content in equilibrium at 20 °C can be described with the sorption isotherm in Fig. 16.

The sorption isotherm was measured using a dual vapor gravimetric sorption analyzer DVS Resolution (Surface Measurements Systems Ltd., United Kingdom). The Brunauer–Emmett–Teller model [36], shown in Equation (12), is fit to experimental measurements. X_{db} is the water loading, m_m refers to the monolayer value, which is the quantity of water molecules present in a single layer on the surface, α_w refers to the water activity and n is a fitting parameter:

$$X_{db} = m_m \frac{n \alpha_w}{(1 - \alpha_w)(1 + (n - 1)\alpha_w)} \tag{12}$$

Lab scale fluidized bed

It is assumed that the particle bed is well mixed and their moisture is homogenously distributed. This is confirmed by comparing the moisture content of the last sample with samples from the entire particle bed. The temperature sensor is positioned at a similar bed height as the microwave sensor at about 5 cm. The temperature in the particle bed is homogeneously distributed. Deviations of less than 1 °C are measured when comparing the temperature sensor of the fluidized bed at a height of 12 cm with a second temperature sensor of the moisture probe at a height and depth of 5 cm (data not shown). These small temperature differences confirm the assumption of a homogeneously distributed bed.

Microwave sensor

In order to examine the measurements dependence on the particle position two experimental setups are used as shown in Fig. 17 and Fig. 18: the (i) first setup allows to examine the effect of the distance perpendicular to the sensor and the (ii) second setup allows to investigate the effect of the distance from the sensor center parallel to the sensor tip while maintaining contact with the particles.

The investigated particle positions inside the measurement volume are numbered from 1 to 7.

The maximum penetration depth of the sensor is about 1.5 cm into the bed normal to the sensor tip. This is determined by approaching the sensor tip normal to the sensor tip until a signal is retrieved as shown in Fig. 17. In Fig. 19 the impact of the distance perpendicular to the sensor tip is

displayed for the initial and agglomerated powder at 2.3 and 5.6 GHz. The moisture signal is clearly influenced by the distance between the solid and the sensor tip in all four cases. In case of the initial powder at 2.3 GHz the measurement is independent of the measurement volume if the sensor plane to particle distance is below a certain threshold at 2.3 GHz. The signal fluctuations of the initial and the agglomerated powder increase with increasing distance. At 5.6 GHz there is a clear increase of the signal with increasing distance for both powders. This means that the measurement volume does not have to be filled completely, but material needs to be rather close to the sensor tip to achieve reproducible and distance independent measurements at 2.3 GHz while at 5.6 GHz the signal converges to the signal at direct contact with the sensor.

The measurement is independent of the particle position parallel to the sensor plane in case of agglomerated powder at all frequencies. This is examined by approaching the measurement volume from the side of the probe as shown in Fig. 18. The results are shown in Fig. 20.

The device can determine the moisture content independent of the mass, which is a function of bulk density due to a constant measurement volume. Two samples are conditioned, one with fine initial powder and a second coarse agglomerated powder produced in the fluidized bed with bulk densities of 550 kg/m^3 and 270 kg/m^3 respectively. The two samples have a moisture content of 10.08 wt% and 9.88 wt% for fine and agglomerated material respectively. The measured MW moisture signals at 2.3 GHz are 0.297 and 0.288 with a standard deviation of 0.05 % and 0.23 % respectively. The measured MW moisture signal at 5.6 GHz are 0.532 and 0.528 with a standard deviation of 0.11 % and 0.14 % respectively. This shows that the MW sensor can measure the moisture content independent of the bulk density at both frequencies.

The device corrects for the change in resonance frequency caused by sensor hull expansion due to different temperatures. The reference resonance frequency in an empty state is set before every experiment. Prior to the adjustment the sensor is preheated as close as possible to the process temperature. The inlet temperature was chosen to approximate the temperature in the process chamber since the process temperature depends on multiple factors such as inlet temperature, inlet air flow rate, bed mass, initial particle moisture content, liquid spray flow rate and others.

Gravimetric method

A precision balance is used to determine the granule moisture content of the samples of about 1 g offline. The samples are weighted before and after drying. The moisture content can then be determined using Equation (13). The samples are dried in the oven for 5 days at 110 °C. The samples are spread in the container to create a thin layer to accelerate drying. The method is compared to an established moisture analyzer. The measurements coincide with moisture analyzer EM 120-HR (Precisa Gravimetrics AG, Germany):

$$x_{wb} = \frac{m_{wet} - m_{dry}}{m_{wet}} * 100 \tag{13}$$

Design of experiment

The process parameters of all experiments are listed in Table 4.

Calibration

The contour plot of the microwave moisture signal at 5.6 GHz is shown in Fig. 21.
The contour plot of the microwave density signal at 2.3 GHz is shown in Fig. 22.
The contour plot of the microwave density signal at 5.6 GHz is shown in Fig. 23.
The parity plot of the CFB calibration applied to the IFB dataset is shown in Fig. 24.
The parity plot of the IFB calibration applied to the CFB dataset is shown in Fig. 25.

Feature selection

The heat map of the Spearman coefficients of the different input parameters for feature selection is shown Fig. 26.
The histograms of input parameters for feature selection are shown in Fig. 27.
The input parameters and the corresponding Pearson and Spearman coefficient for feature selection are shown in Table 5.

Appendix B. Supplementary data

Supplementary data to this article can be found online at https://doi.org/10.1016/j.cej.2024.156053.

References

[1] S. Heinrich, M. Peglow, M. Ihlow, L. Mörl, Particle population modeling in fluidized bed-spray granulation—analysis of the steady state and unsteady behavior, Powder Technol. 130 (1–3) (2003) 154–161, https://doi.org/10.1016/S0032-5910(02)00259-0.
[2] B. Wang, H. Li, J. Xiang, J. Zheng, J. Wang, Fabrication of agglomerated lactose using fluidized bed for good compressibility, J. Nanomater. 2021 (2021) 1–6, https://doi.org/10.1155/2021/9918847.
[3] H. Yuksel, N. Dirim, Agglomeration process in the fluidized bed, the effecting parameters and some applications, Hrvatski Časopis Za Prehrambenu Tehnologiju, Biotehnologiju i Nutricionizam 13 (3–4) (2018) 159–163, https://doi.org/10.31895/hcptbn.13.3-4.10.
[4] S. Shanmugam, Granulation techniques and technologies: recent progresses, Bioimpacts 5 (1) (2017) 55–63, https://doi.org/10.15171/bi.2015.04.
[5] A.A. Ouazzou, Y.M. Harshe, V. Meunier, J.H. Finke, S. Heinrich, Influence of Process Parameters and Particle Size Distribution on Mechanical Properties of Tablets, Chem.-Ing.-Tech. 95 (1–2) (2023) 168–177, https://doi.org/10.1002/cite.202200157.
[6] B. Rambali, L. Baert, D.L. Massart, Using experimental design to optimize the process parameters in fluidized bed granulation on a semi-full scale, Int. J. Pharm. 220 (1–2) (2001) 149–160, https://doi.org/10.1016/S0378-5173(01)00658-5.
[7] C. Avilés-Avilés, E. Dumoulin, C. Turchiuli, Fluidised bed agglomeration of particles with different glass transition temperatures, Powder Technol. 270 (2015) 445–452, https://doi.org/10.1016/j.powtec.2014.03.026.
[8] M. Askarishahi, M. Salehi, S. Radl, Full-physics simulations of spray-particle interaction in a bubbling fluidized bed, AIChE J 63 (7) (2017) 2569–2587, https://doi.org/10.1002/aic.15616.
[9] M. Askarishahi, M.-S. Salehi, S. Radl, Two-fluid-model-based full physics simulations of mixing in noncohesive wet fluidized beds, Ind. Eng. Chem. Res. 58 (27) (2019) 12323–12346, https://doi.org/10.1021/acs.iecr.9b01344.

[10] K. Terrazas-Velarde, M. Peglow, E. Tsotsas, Kinetics of fluidized bed spray agglomeration for compact and porous particles, Chem. Eng. Sci. 66 (9) (2011) 1866–1878, https://doi.org/10.1016/j.ces.2011.01.037.
[11] K.A. Mehta, G.S. Rekhi, D.M. Parikh, Handbook of Pharmaceutical Granulation Technology, CRC Press (2005), https://doi.org/10.1201/9780849354953.
[12] S. Palzer, Influence of material properties on the agglomeration of water-soluble amorphous particles, Powder Technol. 189 (2) (2009) 318–326, https://doi.org/10.1016/j.powtec.2008.04.034.
[13] L. Fries, J. Dupas, M. Bellamy-Descamps, J. Osborne, A.D. Salman, S. Palzer, Bonding regime map for roller compaction of amorphous particles, Powder Technol. 341 (2019) 51–58, https://doi.org/10.1016/j.powtec.2018.02.055.
[14] U.S. Food and Drug Administration. (2004). *Guidance for Industry: PAT - A framework for innovative pharmaceutical development, manufacturing and quality assurance*. https://www.fda.gov/regulatory-information/search-fda-guidance-documents/pat-framework-innovative-pharmaceutical-development-manufacturing-and-quality-assurance.
[15] C. Buschmüller, W. Wiedey, C. Döscher, J. Dressler, J. Breitkreutz, In-line monitoring of granule moisture in fluidized-bed dryers using microwave resonance technology, Eur. J. Pharm. Biopharm. 69 (1) (2008) 380–387, https://doi.org/10.1016/j.ejpb.2007.09.014.
[16] L. Gradinarsky, H. Brage, B. Lagerholm, I.N. Björn, S. Folestad, In situ monitoring and control of moisture content in pharmaceutical powder processes using an open-ended coaxial probe, Meas. Sci. Technol. 17 (7) (2006) 1847–1853, https://doi.org/10.1088/0957-0233/17/7/024.
[17] Kocsis, L., Schlemm, U., Mellmann, J., & Farkas, I. (2008). On-line microwave measurement of the moisture content of wheat. *IFAC Proceedings Volumes (IFAC-PapersOnline)*, *17*(1 PART 1). Doi: 10.3182/20080706-5-KR-1001.4032.
[18] V. Loureno, T. Herdling, G. Reich, J.C. Menezes, D. Lochmann, Combining microwave resonance technology to multivariate data analysis as a novel PAT tool to improve process understanding in fluid bed granulation, Eur. J. Pharm. Biopharm. 78 (3) (2011) 513–521, https://doi.org/10.1016/j.ejpb.2011.02.008.
[19] J. Peters, K. Bartscher, C. Döscher, W. Taute, M. Höft, R. Knöchel, J. Breitkreutz, In-line moisture monitoring in fluidized bed granulation using a novel multi-resonance microwave sensor, Talanta 170 (2017) 369–376, https://doi.org/10.1016/j.talanta.2017.03.105.
[20] J. Peters, W. Taute, K. Bartscher, C. Döscher, M. Höft, R. Knöchel, J. Breitkreutz, Design, development and method validation of a novel multi-resonance microwave sensor for moisture measurement, Anal. Chim. Acta 961 (2017) 119–127, https://doi.org/10.1016/j.aca.2017.01.021.
[21] J. Peters, W. Taute, C. Döscher, R. Meier, M. Höft, R. Knöchel, J. Breitkreutz, From laboratory- to pilot-scale: moisture monitoring in fluidized bed granulation by a novel microwave sensor using multivariate calibration approaches, Drug Dev. Ind. Pharm. 44 (6) (2018) 961–968, https://doi.org/10.1080/03639045.2018.1425427.
[22] J.M. Simkoff, F. Lejarza, M.T. Kelley, C. Tsay, M. Baldea, Process control and energy efficiency, Ann. Rev. Chem. Biomolecul. Eng. 11 (1) (2020) 423–445, https://doi.org/10.1146/annurev-chembioeng-092319-083227.
[23] S. Trabelsi, A.W. Krazsewski, S.O. Nelson, New density-independent calibration function for microwave sensing of moisture content in particulate materials, IEEE Trans. Instrum. Meas. 47 (3) (1998) 613–622, https://doi.org/10.1109/19.744310.
[24] M. Kent, Simultaneous determination of composition and other material properties by using microwave sensors, Sensors Update 7 (1) (2000) 3–25, https://doi.org/10.1002/1616-8984(200001)7:1<3::AID-SEUP3>3.0.CO;2-0.
[25] F. Daschner, R. Knöchel, Dielectric microwave sensors with multivariate calibration, Adv. Radio Sci. 1 (2003) 9–13, https://doi.org/10.5194/ars-1-9-2003.
[26] S. Trabelsi, A.W. Kraszewski, S.O. Nelson, New calibration technique for microwave moisture sensors, IEEE Trans. Instrum. Meas. 50 (4) (2001) 877–881, https://doi.org/10.1109/19.948292.
[27] Y. Roos, M. Karel, Plasticizing effect of water on thermal behavior and crystallization of amorphous food models, J. Food Sci. 56 (1) (1991) 38–43, https://doi.org/10.1111/j.1365-2621.1991.tb07970.x.
[28] Y. Roos, M. Karel, Phase transitions of mixtures of amorphous polysaccharides and sugars, Biotechnol. Prog. 7 (1) (1991) 49–53, https://doi.org/10.1021/bp00007a008.
[29] S. Palzer, The effect of glass transition on the desired and undesired agglomeration of amorphous food powders, Chem. Eng. Sci. 60 (14) (2005) 3959–3968, https://doi.org/10.1016/j.ces.2005.02.015.
[30] Palzer, S. (2007). *Chapter 13 Agglomeration of dehydrated consumer foods* (pp. 591–671). Doi: 10.1016/S0167-3785(07)80048-0.
[31] K. Kramm, M. Orth, A. Teiwes, J.C. Kammerhofer, V. Meunier, S. Pietsch-Braune, S. Heinrich, Influence of nozzle parameters on spray pattern and droplet characteristics for a two-fluid nozzle, Chem. Ing. Tech. 95 (1–2) (2023) 151–159, https://doi.org/10.1002/cite.202200152.
[32] J. Tausendschön, G. Stöckl, S. Radl, Machine Learning for heat radiation modeling of bi- and polydisperse particle systems including walls, Particuology 74 (2023) 119–140, https://doi.org/10.1016/j.partic.2022.05.011.
[33] J. Tausendschön, S. Radl, Deep neural network-based heat radiation modelling between particles and between walls and particles, Int. J. Heat Mass Transf. 177 (2021) 121557, https://doi.org/10.1016/j.ijheatmasstransfer.2021.121557.
[34] C. Vanaret, P. Seufert, J. Schwientek, G. Karpov, G. Ryzhakov, I. Oseledets, N. Asprion, M. Bortz, Two-phase approaches to optimal model-based design of experiments: how many experiments and which ones? Comput. Chem. Eng. 146 (2021) 107218 https://doi.org/10.1016/j.compchemeng.2020.107218.
[35] M. Gordon, J.S. Taylor, Ideal copolymers and the second-order transitions of synthetic rubbers. i. non-crystalline copolymers, J. Appl. Chem. 2 (9) (1952) 493–500, https://doi.org/10.1002/jctb.5010020901.
[36] S. Brunauer, P.H. Emmett, E. Teller, Adsorption of gases in multimolecular layers, J. Am. Chem. Soc. 60 (2) (1938) 309–319, https://doi.org/10.1021/ja01269a023.